Die für Transmissionsberechnungen benötigte Größe der gesamten optischen Weglänge L_{0r} erhält man beim gekrümmten Lichtleiter aus der Gesamtzahl N_r der Reflexionen am Kern/Mantel-Übergang

$$L_{0r} \approx N_r \cdot l_{0r} \tag{20}$$

mit $N_r = L_r/l_r$, wobei L_r die geometrische Krümmungslänge des Lichtleiters ist.

6. Zusammenfassung und Schlußfolgerungen

Bei der Ableitung der Aperturverhältnisse der Reflexionslängen und der Zahl der Reflexionen beim gekrümmten Lichtleiter sind zwei Bereiche zu unterscheiden: Ein Bereich, in dem die sukzessiven Reflexionen alternierend am Innen- und Außenbogen erfolgen und ein zweiter Bereich, in dem nur noch am Außenbogen Reflexionen vorkommen. Die Bereichstrennung erfolgt durch den Grenzkrümmungsradius, der selbst wieder eine Funktion insbesondere der Strahleintrittshöhe am Lichtleiterkrümmungsbeginn ist. Die Krümmungsverhältnisse bestimmen die seitliche Abstrahlung und damit den Transmissionsverlust bei idealen Lichtleitern. Hierfür läßt sich ein minimaler optisch erlaubter Krümmungsradius angeben. In Abhängigkeit von der Strahleintrittshöhe zeigt sich, daß der Bereich des Außenbogens des Lichtleiters der entscheidende Bereich für die Lichtleitung insbesondere um extrem kleine Krümmungen ist. Dies kommt auch darin zum Ausdruck, daß die maximal erlaubten Einfallswinkel Funktionen der Einfallshöhe eines Meridionalstrahls sind und zu einer zur optischen Lichtleiterachse unsymmetrischen Apertur führen.

Die für theoretische Transmissionsuntersuchungen maßgeblichen optischen Reflexionslängen und Reflexionszahlen zeigen eine komplizierte Abhängigkeit von Materialgrößen, Materialabmessungen, Einfallswinkel und Einfallshöhe. Die numerische Auswertung zeigt, daß es auch hier Bereiche gibt, in denen die Werte beim gekrümmten Lichtleiter größer oder kleiner als im entsprechenden geraden Lichtleiter sind. Eine a priori Überlegenheit des geraden Lichtleiters gegenüber dem gekrümmten Lichtleiter gibt es folglich bei idealer Totalreflexion an der Kern/Mantel-Grenzfläche nicht.

Literatur

[1] Reidenbach, H.-D.; Bodem, F.; Frühmorgen, P.; Brand, H.; Demling, L.: Endoscopy **7** (1975) 196.
[2] Reidenbach, H.-D.: Theoretische und experimentelle Untersuchungen an Kunststofflichtleitern zur Leistungsübertragung. Dissertation, FA Universität Erlangen-Nürnberg, 1976.
[3] Allan, W.B.: Fibre Optics – Theory and Practice. Plenum Press, London (1973).
[4] Kapany, N.S.: Optical Systems with Flexible Axes. Ph. D. Thesis, Imperial College, London, Jan. 1955.
[5] Kapany, N.S.: Fiber Optics – Principles and Applications. Academic Press, New York (1967).
[6] Lisitsa, M.P.; Berezhinskii, L.I.; Valakh, M.Ya.: Fiber Optics. Wiley, Halstead Press, New York (1972) (Volokonnaya optika: Tekhnika, Kiew 1968).
[7] Kapany, N.S.: J. Opt. Soc. Am. **47** (1957) 413.

Optik 47 (1977) No. 4, 437–452 © Wissenschaftliche Verlagsgesellschaft mbH, Stuttgart

High resolution electron microscopy of phase objects: Observation of small holes and steps on graphite crystals

Sumio Iijima

Department of Physics
Arizona State University
Tempe, Arizona 85281 USA

Received 27 October 1976

Abstract

By means of phase contrast electron microscopy, extremely small holes with diameters of several angstroms that were formed on the surface of a thin film of a graphite single crystal by electron beam irradiation in the electron microscope, were observed. These holes grew as atomic steps on the surface of a graphite crystal with an elongated exposure to the electron beam. We constructed various models of holes and their image intensities were calculated by using the phase object approximation. The calculations confirmed that the holes resulting from removal of 4–16 carbon atoms from the surface of a graphite crystal give sufficient phase contrast to be observed under practical conditions of the electron microscope.

Inhalt

Hochauflösende Elektronenmikroskopie von Phasenobjekten. Beobachtung kleiner Löcher und Stufen an Graphitkristallen. Mit Phasenkontrast-Elektronenmikroskopie werden extrem kleine Löcher beobachtet, sie haben Durchmesser von einigen Angström und wurden auf der Oberfläche von Graphitkristallen durch Elektronenbeschuß gebildet. Diese Löcher wuchsen über atomare Stufen während der Einwirkung des Elektronenstrahls. Wir entwickelten mehrere Modelle für diese Löcher und berechneten ihre Bildintensitäten mit der Phasenobjekt-Approximation. Die Rechnungen zeigen, daß beobachtbare Löcher entstehen, wenn 4–16 Kohlenstoffatome aus der Oberfläche eines Graphitkristalls entfernt werden.

1. Introduction

We have developed a technique to prepare thin single crystalline films of graphite with thicknesses of down to 20 Å for use as supporting films for high resolution electron microscopy [1]. The surfaces of the films inherently contain step structures which have been formed during thinning the films. They became visible in the images taken by defocussing the objective lens. Therefore image contrast at regions of the steps can be interpreted in terms of phase object and the heights of the steps were thought to be only a few atomic

layers of hexagonal networks of carbon atoms. During testing of the films as supports, we found also that the films were etched by an electron beam irradiation to form similar steps on the surface of the films.

In the present paper we shall discuss imaging of small holes or pits that are formed by removing only 4–16 carbon atoms from the surface of the graphite films. The observed image contrasts of small holes are compared with those theoretically calculated from some model structures by phase object approximation.

2. Experimental observation

A thin graphite single crystalline film is prepared in the electron microscope by etching the surface of the film with an intense electron beam irradiation, inducing a reaction between the carbon and some added tungsten trioxides [1]. The intense electron beam was obtained by removing the condenser aperture. Subsequently the films were observed under the normal imaging conditions for bright field high resolution microscopy by a JEOL-100B electron microscope. The direct magnification was × 500,000. The size of the objective aperture was 0.44 $Å^{-1}$ in reciprocal space. With this aperture {1000} reflections of graphite crystals which correspond to 0.48 $Å^{-1}$ are excluded and only the transmitted beam contributes to the image. Electron images were recorded on Kodak Electron Image Plates which were developed in D-19 for eight minutes. The optical density of the negatives was within a range of $1.6 \sim 2.0$. The original copies for photo publication were printed on photo papers of No. 4.

In high resolution work it is always required to know defocus values accurately. A simple method to determine defocus values is to observe an amorphous carbon film which is mounted on the tilted specimen holder at 45 degrees to the direction of the incident beam. Sequences of two images of the film are recorded with this holder in such a way that the first image has minimum contrast (so-called near-in-focus image) in a band across the negative and then a second image is taken by changing focus by a known number of steps (denoted by N) in the objective lens current control knobs of the microscope. On the second image the band showing minimum contrast has been shifted by a certain distance (denoted by X) perpendicularly to the band in the first image. The magnification of the images is calibrated by recording simultaneously lattice dringes of graphatized carbon black collected on the same amorphous carbon film. The value X/N then gives an amount of defocus corresponding to one step of the focussing control knobs. Error of this method was within 5%. It is noted that since a focus giving minimum contrast for the amorphous carbon film does not represent the in-focus value because of spherical aberration, the measured values are on a relative scale. In the present experiment we assume that a minimal contrast image of an edge of the film of graphite crystal occurs at — 250 Å.

Figure 1 shows a series of bright field images of a film taken under the condition of the optimum focus of — 925 Å. These images were recorded successively with an interval of about 3 minutes. The dark objects which

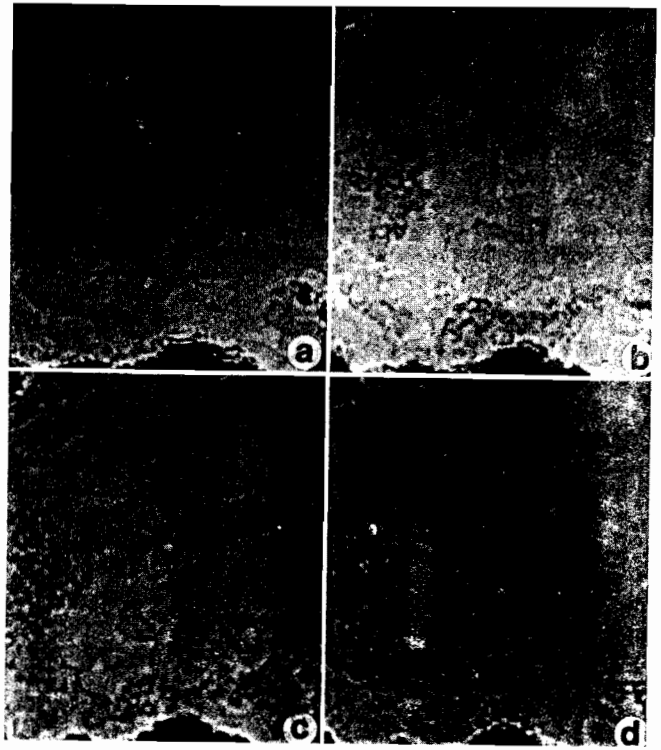

Fig. 1. A sequence of images of an extremely thin crystal of carbon graphite with an extension of electron beam irradiation, showing growth of steps on the surface of the crystal. Interval of exposure time to the electron beam is three minutes. The images were recorded under the condition of optimum focus ($\varepsilon = -925$ Å). A region shown by an arrow for instance becomes larger with an exposure time to grow as a step.

also appear in the following pictures are metallic tungsten that were by-products of the reduction reaction of WO_3 with carbon during thinning of the films. In all images we can recognize very fine spots with 5–10 Å in diameter and contour lines which mostly enclose areas, forming loops. The loops expand with an extended exposure of electron beam irradiation. For instance, a small spot with a diameter of 10 Å marked by an arrow in Figure 1 a becomes larger and grows as a loop in the following images. Many similar spots with lighter contrast have been developed in Figure 1 d which resemble that in Figure 1 a and therefore they will expand with a further extension of the irradiaton. These small spots seem to be therefore nucleations of the contour lines or loops.

Since the contour lines and the small spots with lighter contrast have disappeared when they were imaged under the condition of the near in-focus,

the image contrast for them may result from phase contrast of thin objects. The thickness of the films were so small, estimated to be 20–50 Å, that the assumption made above would be valid. Immediately we can expect that such thin objects causing the contour lines would be step structures with a few atomic layers on the surface. Then the question arises as to what is the height of the steps and what is the structure making such small spots visible.

For these questions, we made a further observation on the fine spots. Figure 2 shows a pair of the images of a graphite film taken at the beginning of the electron beam irradiation (Figure 2a) and after five minutes irradiation (Figure 2b). In these pictures we can see lattice fringes corresponding to the

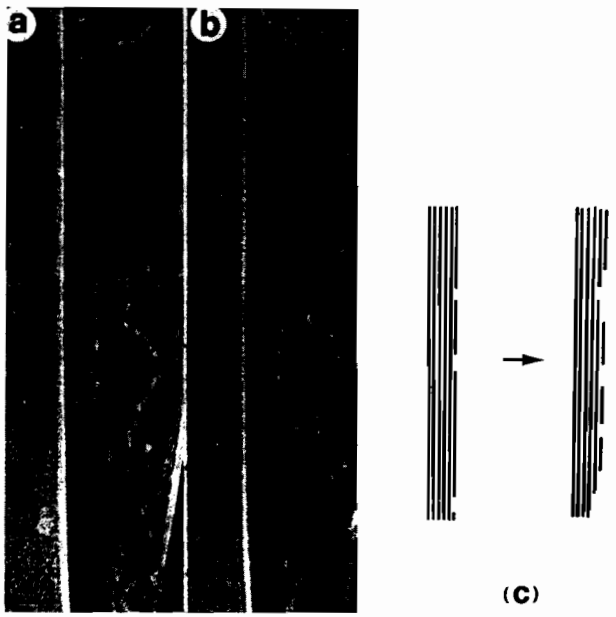

Fig. 2. A pair of images of an edge of a thin film of a graphite crystal (a) before and (b) after electron beam irradiation. The edge of the film is curled up so that the sheets of carbon atom networks are parallel to the direction of the incident electron beam. The number of fringes serves to estimate the crystal thickness. Regions arrowed in (a) suggest that holes shown in Fig. 1 occur only with a single atomic step and become wider and deeper in (b). (c) A schematic representation of growth of atomic steps observed in (a) and (b).

c-spacing of 3.8 Å near the film edge; these fringes resemble those of graphitized carbon blacks. This means that the edge of the film is curled up such that the c-axis of the graphite crystal becomes almost perpendicular to the incident beam, while the other region (on the right hand side of each image)

remains with the c-axis nearly parallel to the beam. Incidentally from this picture we can deduce the thickness of the film by counting the number of the lattice fringes appearing in the edge of the film. It turns out to be 26.7 Å (corresponding to 7 layers) at near the bottom of the image and 19 Å (corresponding to 5 layers) at the top. In Figure 2a the edge of the film is smooth except for occasional erosions on the surface (arrowed) and small spots similar to those in Figure 1 are also seen on the right hand side of the image. In Figure 2b the edge forms many steps with height of only a single atomic layer (3.8 Å). These pairs of the photographs suggest therefore that at the beginning of the irradiation small holes probably with a depth of a single atomic layer are formed on the top surface and they grow progressively larger, mostly two-dimensionally, within a few top layers. The growth of the holes is schematically illustrated in Figure 2c. This observation supports our interpretation of the images of the small spots and the loops shown in Figure 1.

In order to find how small the holes are that can be detected in bright field electron microscope images, we examined properties of the image contrast of the small spots. Figure 3 shows a through-focus series of images of a thin graphite crystal which has not been electron irradiated intensely except that the one shown in Figure 3f was recorded after prolonged electron beam irradiation. Amounts of defocus for these images are: (a) + 425 Å, (b) — 250 Å, (c) — 925 Å, (d) — 1600 Å, (e) — 2275 Å and (f) — 925 Å. The edge of the film is seen at the bottom of each image, showing Fresnel diffraction-like edge images due to defocus of the objective lens (marked by big arrow). The visibility as well as the widths of the fringes can be interpreted in terms of phase contrast and will be utilized to estimate the thickness of the films. The same analogy can be applied to the visibility of fringe images generated near the steps on the surface of the film and the height of the steps can be estimated. This will be reported soon.

Similar small spots with lighter contrast than for those observed in Figure 1a and 1d are seen in the optimum focus image (Figure 3c). The sizes of the spots are 4 ~ 7 Å in diameter and some of those are marked by arrows. The image contrasts of the spots in Figure 3c are reversed as dark spots in the image taken at over-focus of + 425 Å (Figure 3a) and become invisible at near in-focus of — 250 Å (Figure 3b). The sizes of the spots become larger by further defocussing the objective lens to — 1600 Å and — 2275 Å (Figure 3d and 3e). With a prolonged electron irradiation the number of the spots is increased and some of those grow larger as we described in relation to Figure 1 (Figure 3f). Figure 3f is the optimum focus image. Accordingly we suspect that these small spots observed in the images of a thin graphite film are nucleations of atomic steps to grow on the surface of the film.

Another finding from the series of pictures, although not directly related to the present subject, is that many distinct dark spots with sizes of 4–10 Å in diameter are seen and their contrasts are reversed in the over-focussed image (Figure 3a). The smallest dark spots in the optimum focus image (Figure 3c) are 3 ~ 4 Å in diameter. It is noted that the sharpest images of the dark spots as well as the lighter spots and the edge of the film described before are always attained in the optimum focus image. An enlarged image of Figure 3c is

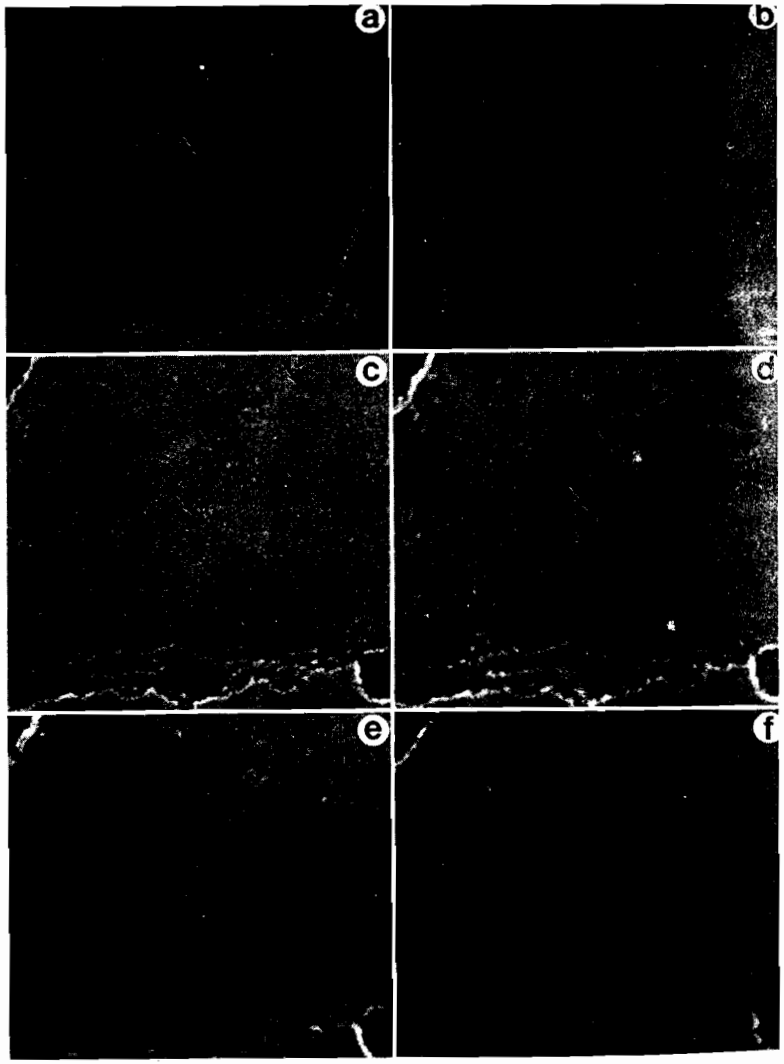

Fig. 3. A through-focus series of images of a very thin film of a graphite crystal on the surface of which very fine holes have been formed with electron beam irradiation. Defocus values were (a) — 425 Å, (b) — 250 Å, (c) — 925 Å, (d) — 1600 Å, (e) —2275 Å and (f) — 925 Å. The image in (f) recorded after a longer electron beam exposure showed growths of steps. The optimum focus image (c) shows smallest spot (several Angstroms in diameter) with lighter contrast (arrowed) among the other under-focused images. Their contrasts are reversed in the over-focused image (a) and disappeared in the near in-focus image (b) and therefore the images of these holes are interpreted as nearly phase objects.

reproduced in Figure 4. The dark spots are mostly located on the contour lines (on the left hand side of the image) which we thought as the steps of graphite layers formed during thinning the surface. As we mentioned earlier larger black objects in the image are crystals of metallic tungsten and therefore it is reasonable that fine metallic tungsten particles are also produced.

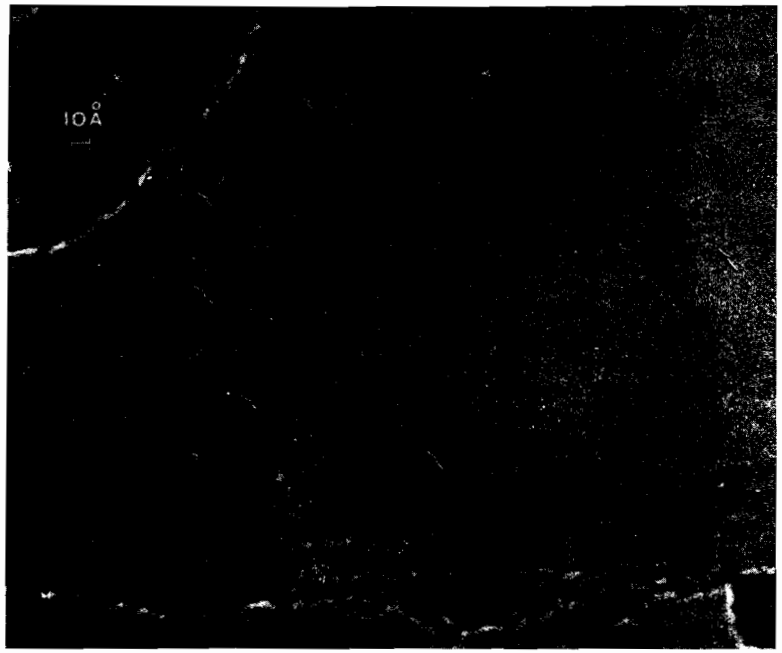

Fig. 4. An enlarged image of Fig. 3c. Dark spots arrowed are supposed to be the images of single tungsten atoms.

They have been eventually trapped at some irregularities of the surface such as steps. Since they do not move during observation the tungsten atoms in these particles might be firmly bonded with carbon atoms on the surface. In other words they may not be metallic tungsten but tungsten carbide.

The smallest size of the particles indicated by arrows is about 4 Å in diameter. The image contrast of these particles is less than for other dark spots. Moreover it is surprising that these particles have almost the same size and contrast. It is highly probable therefore that the smallest particles might be single tungsten atoms. Justification of this postulation should be achieved by comparing experimental images of the particles with theoretically calculated images. This will be reported in the succeeding paper.

3. Image contrast of the small holes

In the preceding section we described experimental observations of image contrast of small holes formed on the surface of graphite film by means of an electron beam irradiation. The dimensions of the holes are so small that they might be created by removing only several carbon atoms from the surface of graphite crystal. The arrangements of carbon atoms around such holes therefore can be readily known from the original crystal structure of graphite by assuming that there is no appreciable displacements of the atoms near the holes. Then the image contrast arising from such small holes can be calculated by the theory of imaging of phase objects. In this section, to justify the experimental results described in Section 2, we discuss image contrasts theoretically calculated for various model structures of the holes. In particular it is aimed to find how small are the holes that can be observed under the practical imaging conditions of high resolution microscopy.

3.1. Models for the holes

The crystal structure of an ideal single crystal of graphite consists of sheets of carbon atoms with a hexagonal arrangement. Within the basal plane the individual sheets are displaced alternatively by $a/\sqrt{3}$ along the $\langle 210 \rangle$ of hexagonal cell. The structure of the graphite crystal is shown schematically in Figure 5a where black dots represent carbon atoms and half of the orthorhombic unit cell is shown by dotted lines. The distance between the two neighboring sheets is 3.35 Å. The models used for the calculations of image intensities are constructed by removing a certain number of carbon atoms from one of the two layers or from both layers. Five models constructed in this way are shown in Figure 5b–f. They are:

(b) Four carbon atoms removed from the bottom layer,
(c) Six carbon atoms (one hexagon) removed from the top layer,
(d) Twelve carbon atoms removed from the top layer,
(e) Ten carbon atoms removed; six from the top layer and four from the bottom,
(f) Sixteen carbon atoms removed; twelve from the top layer and four from the bottom.

As we describe next, the calculations of image contrasts for these model structures are made by the phase object approximation in which a potential of an object is projected on a plane along the direction of the incident beam and therefore three dimensional arrangements of the carbon atoms in the models may not be important.

3.2. Calculation of the image intensities

Since we assume that the thickness of the films containing missing carbon atoms is just one unit cell of graphite crystal (6.696 Å), it is a reasonable assumption that the films are perfect phase objects and a phase object

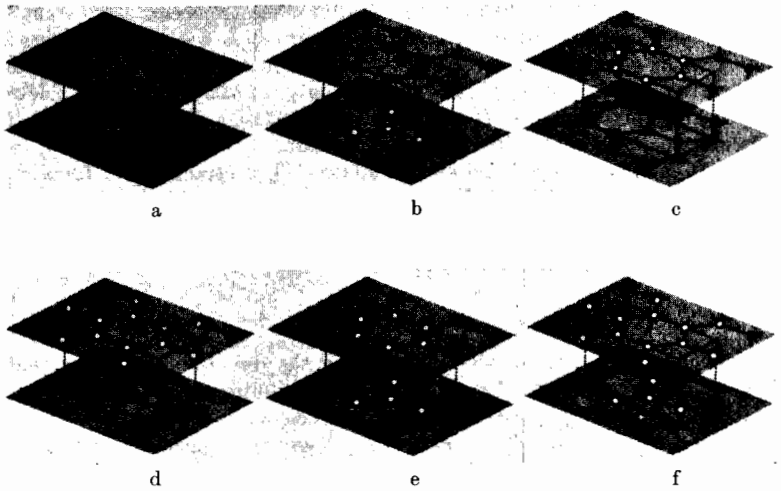

Fig. 5. Models used for the calculation of the images of small holes on the surface of a graphite crystal. (a) A perfect crystal of graphite. (b) Three, (c) Six atoms, (d) Twelve atoms (e) Ten and (f) Sixteen carbon atoms are removed.

approximation will be sufficient for calculating image intensities of the holes. In the calculation, presence of the layers beneath the first two layers which contain the holes has not been taken into account although the thickness of the films observed in the present experiment is in a range of 20–50 Å. The effect of these additional layers on the image contrast of the holes will be quite small and can be ignored for the following reasons.

The experimental images of the films were recorded by using only transmitted beams and therefore there will be no contributions to the image contrast of the holes from the additional layers except for an increase in uniform background contrast which will be superimposed on the images of the holes. The background contrast results mainly from amplitude contrast produced by excluding Bragg reflections, arising from the perfect region of graphite crystal that is located under the layers with holes, by use of the objective aperture. As we mentioned elsewhere [1] however the intensity of the transmitted beam passing through a very thin film of graphite crystal of less than 50 Å, which is the case of our films used in the present experiment, is decreased very slightly. For instance, the intensity of the incident beam for the thickness of 50 Å falls off by 5%. This means that any blurring effect on the images of the holes due to the substrate film may be quite small.

Another effect on the background intensity to be considered will be from thermal diffuse scattering associated with the atoms in the substrate film. The wave amplitudes of the thermal diffuse scattering are zero at the origin of the reciprocal space and gradually increase at increasing scattering angles.

This means that some of the thermally scattered electrons can pass through the objective aperture and contribute to a slight increase in the background intensity. As a result, the overall background intensity becomes a little higher than that for the amplitude contrast only. In other words, the thickness of the film becomes effectively smaller than the actual one. This is favorable to observing objects sitting on the film.

According to the phase object approximation [2], the transmission function of an object can be written as

$$q(\boldsymbol{r}) = \exp\left[-i\sigma\varphi(\boldsymbol{r})\right] \tag{1}$$

where $\sigma = \dfrac{\pi}{\lambda E}$, E is accelerating voltage, λ is an electron wavelength and $\varphi(\boldsymbol{r})$ is a projected potential of the object along the direction of the incident electron wave. To obtain a two-dimensional distribution of a potential $\varphi(\boldsymbol{r})$, we assume an artificial crystal with a large unit cell of $\boldsymbol{a} = 9 \times \boldsymbol{a}_0$, $\boldsymbol{b} = 5 \times \boldsymbol{b}_0$, and $\boldsymbol{c} = \boldsymbol{c}_0$, where $\boldsymbol{a}_0 = 2.456$ Å, $\boldsymbol{b}_0 = 4.254$ Å and $\boldsymbol{c}_0 = 6.696$ Å, corresponding to the dimension of an orthorhombic unit cell of graphite, and as we described in Section 3.1 some of the carbon atoms are removed from this unit cell which contains 360 carbon atoms. To reduce some errors on the image contrast of the holes arising from having such an artificial crystal, it is desirable for sizes of the unit cell to be taken as large as possible. In an extreme case, if we take the unit cell dimensions to infinity, the intensity distribution of diffracted amplitudes in the reciprocal space becomes continuous, which is an exact calculation of a non-periodic object. In practice, however, the number of the sampling points in the unit cell is restricted. Our computer program has 64×64 arrays and therefore a compromised value was chosen as mentioned above. With this unit cell a sampling distance becomes 0.34 Å in both x and y directions which seems to be sufficient for discussing image contrasts with a resolution of around 3 Å. The number of the beams used for the two-dimensional calculations was about 450, varying slightly with the models.

Detailed procedures of calculation of image intensities for crystals have been reported by several workers (for example, Cowley 1975) and will not be repeated here. One thing however should be noted, which has not been considered in the previous literature.

The incident and diffracted wave amplitudes on the back focal plane are given by Fourier transform of equation [1]. These amplitudes are modulated by a physical objective aperture, $A(\boldsymbol{u})$ and by the propagation function (Scherzer transfer function), $\chi(\boldsymbol{u}) = \pi\varepsilon\lambda\boldsymbol{u}^2 - \frac{1}{2}\pi C_s\lambda^3\boldsymbol{u}^4$ due to the amount of defocus (ε) and spherical aberration (C_s). In the present calculations, the effects of chromatic aberration and divergence of the incident beam which have been introduced by Fejes [3] and Anstis and O'Keefe [4] respectively were also taken into consideration. They are expressed as functions $B(\Delta, \boldsymbol{u})$ and $C(\alpha, \Delta, \boldsymbol{u})$ respectively where Δ is the half width of a Gaussian distribution of focus due to chromatic aberration, α is the semi-angle of the incident beam divergence and $\boldsymbol{u}$ is a radial coordinate in reciprocal space.

Corrected amplitude distributions are then expressed as

$$\psi(\boldsymbol{u}) = \mathscr{F}\{\exp\left[-i\varphi(\boldsymbol{r})\right]\} \cdot \exp\left[-i\chi(\boldsymbol{u})\right] \cdot B(\Delta, \boldsymbol{u}) \cdot C(\alpha, \Delta, \boldsymbol{u}). \tag{2}$$

Then the image intensities on the image plane, $I(\boldsymbol{r})$ are obtained through back Fourier transform of equation (2) and expressed as

$$I(\boldsymbol{r}) = \mathscr{F}^{-1}\{\psi(\boldsymbol{u}) * \psi^*(\boldsymbol{u})\} \tag{3}$$

where $*$ represents a convolution operation.

The computer program for the image intensity calculation of crystals by the n-beam multislice method originally written by Fejes [5] and Skarnulis [6] was used for the present calculation with some modifications by assuming the number of slices equal to one.

Data of instrumental parameters used in the calculations are: accelerating voltage 100 kV, spherical aberration constant 1.8 mm, depth of focus due to chromatic aberration 125 Å, incident beam divergence semi-angle 1.4 milliradian, objective aperture size 0.44 Å^{-1} in reciprocal space.

4. Results and discussion

Firstly it was sought to find a condition giving a maximum contrast (darkest contrast in the negatives) at the position of the holes. Series of images of the holes were calculated by changing the amount of defocus and it was found that maximum contrast in the images was obtained by assuming an amount of defocus being — 925 Å. This value was consistent with all models for the holes shown in Figure 5. Those images are so-called optimum focus images, being in accordance with those obtained from a simpler thin phase object approximation. This suggests that image intensities for very thin objects can be given by $I(\boldsymbol{r}) = 1 - 2\sigma\varphi(\boldsymbol{r}) * \mathscr{F}\{\sin\chi(\boldsymbol{u})\}$ and therefore $I(\boldsymbol{r}) \cong 1 - 2\sigma\varphi(\boldsymbol{r})$ for $\sin\chi(\boldsymbol{u}) \cong 1$. Image intensity thus becomes proportional to the projected potential of the object. In the present calculation, we did not use a thin phase object approximation which is a good approximation for image intensity calculated if $\sigma\varphi(\boldsymbol{r}) \ll 1$. This condition can be satisfied sufficiently with our objects of graphite crystal film with a thickness of two layers and thus we can expect almost the same results by using this approximation. Accordingly the optimum focus images calculated here represent approximately the projected potentials of the objects along the direction of the incident beam.

According to Anstis and O'Keefe [4], the modified propagation function of equation (2) has the effect of changing the cut-off frequency given by the function $\exp\{-i\chi(\boldsymbol{u})\}$ and also to damp off the envelope in the higher frequency regions. These effects due to beam divergence and chromatic aberration become more important for imaging of crystals because diffracted wave amplitudes on the back focal plane from crystals are discontinuously

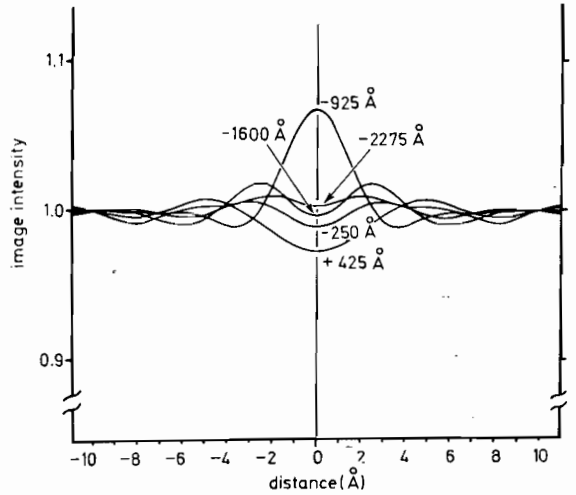

Fig. 6. Image intensity profiles calculated for the holes shown in Fig. 5b at various amounts of defocus.

distributed with various magnitudes but for deviations from perfect crystallinity as in the present case they will result in slight reductions of resolutions and intensities of the images.

Image intensity profiles of through-focus images calculated for the model b where 4 carbon atoms are removed are shown in Figure 6. The increment of focus in the images is 675 Å. This value corresponds to an increment in the focal steps in the experimental images shown in Figure 3 which corresponds to the calibrated value of one step of the fine-coarse knob in our JEM-100B electron microscope. The image contrast for $\varepsilon = -925$ Å is 8.0% and the half peak width is 3.2 Å while contrasts of the other images are less than about 5% which is a minimum value to be recognized. Here we defined the contrast as $I_{max} - I_{min}$ instead of taking I_{min} as unity corresponding to the background intensity I_{AV}. For this model the holes can be observed only in the optimum focus image. The whole through focus image series calculated for model b however do not agree with the experimental images of Figure 3.

Figure 7 shows similar profiles of image intensities for model d where 10 atoms are removed. Figure 8 shows simulated through focus images of this model. The image intensities of the simulated images are not represented in a common intensity scale so that to discuss visibilities of the images, the profiles of the image intensities should be considered. The image of the top left is the potential projected on to the basal plane of the graphite crystal. The darkest regions indicates positions of the carbon atoms and an area with lighter contrast at the center indicates the position where 10 carbon atoms are

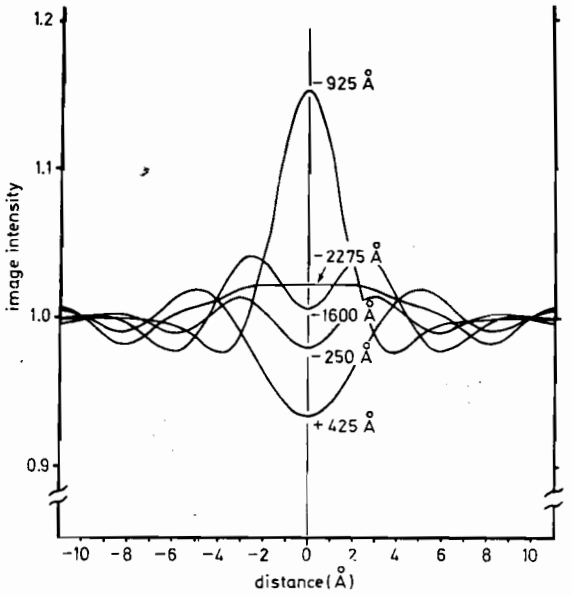

Fig. 7. Image intensity profiles calculated for the holes shown in Fig. 5e at various amounts of defocus.

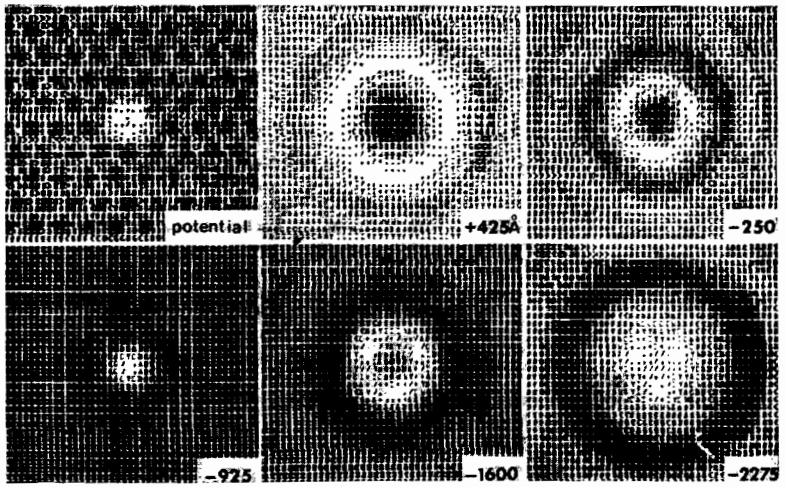

Fig. 8 A simulated through-focus image corresponding to Fig. 7. The image at the top left shows a projected potential of the holes shown in Fig. 5e along the direction of the electron beam.

missing. Full scale of the images are 22.1 Å wide and 21.27 Å high. For this model the image contrast of the optimum focus image of $\varepsilon = -925$ is 17.6% and the half peak width is 3.3 Å and the other images of $\varepsilon = +425$ Å and -1600 Å are approximately more than 5% so that they are all recognizable. The image of $\varepsilon = -1600$ Å has a shallow dip at the center of the hole but it may not be seen because of the small change in contrast as shown in its simulated image in Figure 8. For this reason image contrast and half peak width of such images were measured by ignoring the dips. It is noted that the image of $\varepsilon = +425$ Å has a reversed contrast from those of the others. The image contrasts of $\varepsilon = -250$ Å and -2275 Å however are less than 5% so that they cannot be observed. These result except for the image of $\varepsilon = -2275$ Å are qualitatively consistent with the experimental images of Figure 3. The experimental image corresponding to that of $\varepsilon = -2275$ Å (Figure 3e) in which small holes are even more clearly imaged disagrees with the calculated image. One possible explanation for this is that even though the experimental through-focus series of pictures were recorded as quickly as possible, the growth of the holes due to electron irradiation is inevitable as we showed in Figure 1 and 3f and thus the holes in the image of Figure 3e might have grown larger than those in the other images. If this happened, the present model cannot be applied to the image of Figure 3e. In fact as we describe below, images of the holes which are formed by removing more than 10 carbon atoms have sufficient contrast to be recognized under the same condition of defocussing as -2275 Å.

Contrasts and half peak widths of the images calculated for five models are summarized in Table 1. The contrasts of all optimum focus images whose

Table I

Calculated image contrasts and half-peak widths of various models for the holes on the surface of graphite crystal

	Defocus (Å)				
Models	+ 425	− 250	− 925	− 1600	− 2275
b (4)	3.6 (4.8)*	1.7 (–)	8.0 (3.2)	2.5 (–)	0.7 (–)
c (6)	4.8 (4.8)*	1.6 (–)	9.3 (3.5)	3.5 (8.3)	1.8 (–)
d (10)	8.4 (4.3)*	3.4 (3.0)	17.6 (3.3)	6.3 (8.4)	3.9 (11.8)
e (12)	4.8 (4.8)*	0.6 (–)	7.6 (5.2)	6.8 (6.4)	4.7 (9.0)
f (16)	9.3 (5.0)*	1.4 (–)	15.0 (4.1)	7.6 (8.3)	5.9 (9.3)

Figures in parentheses represent half-width of the peaks – Angstrom unit.
* represents reversed contrasts.
Figures in the "models" column show the number of missing carbon atoms.

image intensity profiles are also shown in Figure 9 are approximately more than 5% and the lowest one is 7.5% for the model d where 12 carbon atoms arranged two-dimensionally are removed. Therefore all holes postulated in the present calculation can be detectable under the condition of optimum focus. On the other hand any images of $\varepsilon = -250$ Å failed to show detectable

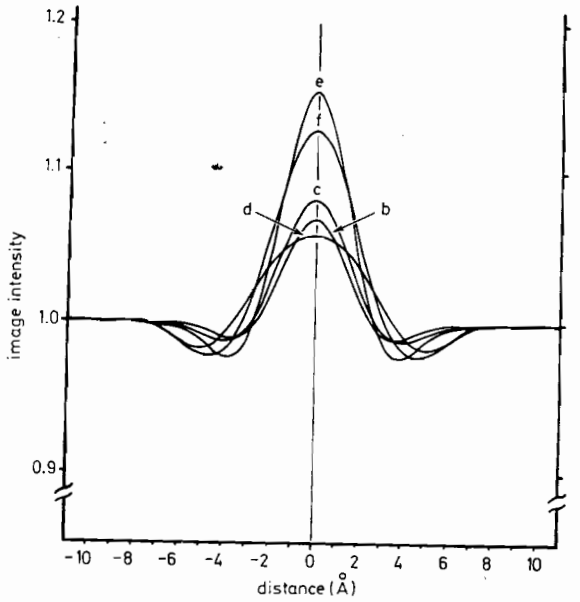

Fig. 9. Image intensity profiles of the optimum focus images ($\varepsilon = -925$ Å) calculated for the five models for the holes shown in Fig. 5.

contrasts. This is not surprising because our objects are nearly perfect phase objects. This result supports validity of our postulate that the amount of defocus giving minimum contrast of an edge of the film of graphite crystal is -250 Å. For the over-focussed images contrasts become nearly half of those of the optimum focus but they still show sharper images of the holes except for that of model b although their contrast are reversed. This result explains the sharper dark sports appearing in Figure 3c.

From comparison of calculated image intensities with the experiments we may conclude that detectable sizes of holes on the surface of graphite crystal correspond to removal of 4–10 carbon atoms.

5. Conclusion

Small holes formed by removal of 4–10 carbon atoms and steps with a single atomic layer on the surface of graphite crystal which take place by electron beam irradiation in the electron microscope have been detected by means of phase object electron microscopy.

Conversely, such phase objects will serve as a standard test object to study image properties of phase objects in terms of electron diffraction and electron optics.

This technique can be applied to investigate very small cavities, inclusions of foreign atoms and surface irregularities occurring at atomic scale inside or on the surface of crystals.

Acknowledgment

I wish to thank Dr. A.J.Skarnulis for permission to use his computer program and also Drs. G.R.Anstis and M.O'Keefe for their modification of the computer program and stimulating discussion through this work. I am grateful to Professor J.M.Cowley for his continuous encouragement. This work was supported by NSF Grant DMR 76-06108.

References

[1] Sumio Iijima, submitted to Micron (1977).
[2] J.M.Cowley, "Diffraction Physics". North-Holland Publishing Co., Amsterdam (1975).
[3] P.L.Fejes, Acra Cryst, in press (1976).
[4] G.R.Anstis and M.O'Keefe, Acta Cryst, to be published (1977).
[5] P.L.Fejes, Ph. D. Thesis of Arizona State University (1973).
[6] A.J.Skarnulis, Ph. D. Thesis of Arizona State University (1975).

Optik 47 (1977) No. 4, 453–467 © Wissenschaftliche Verlagsgesellschaft mbH, Stuttgart

Photometry and partial coherence in electron optics: General relations

P.W.Hawkes

Laboratoire d'Optique Electronique du C.N.R.S., Toulouse*)

Received 29 October 1976

Abstract

The far-zone behaviour of wave fields generated by sources of arbitrary coherence has recently been analysed in detail and generalizations of the traditional radiometric quantities have in consequence been introduced. We derive formulae describing the propagation of these quantities and of various useful second-order correlations between spaces separated by an optical medium. Although we follow the light optical analysis closely, we draw attention to the electron optical relevance of the results wherever appropriate. In a companion paper, the corresponding results for isoplanatic systems will be given; discrete forms of the more important relations will be presented and used to establish invariance and conservation rules.

Inhalt

Photometrie und Teilkohärenz in der Elektronenoptik: Allgemeine Beziehungen. Die Wirkung von Quellen beliebiger Kohärenz im Fernfeld wurde vor kurzem eingehend analysiert, infolge davon wurden Verallgemeinerungen für die traditionellen photometrischen Größen eingeführt. Wir leiten Formeln für die Fortpflanzung dieser Größen ab und für verschiedene nützliche Korrelationen zweiter Ordnung zwischen Räumen, die durch ein optisches Medium getrennt sind. Obwohl wir einer lichtoptischen Analyse folgen, betonen wir die Bedeutung geeigneter Ergebnisse für die Elektronenoptik. In einer weiteren Arbeit werden entsprechende Ergebnisse für isoplanatische Systeme mitgeteilt; bestimmte Formen der wichtigeren Beziehungen werden dargestellt und zur Formulierung von Regeln für Invarianz und Erhaltung verwendet.

1. Introduction

Although the properties of electron sources have been widely studied and the effects of finite source size and wavelength spread on electron image formation have been explored in detail for many illumination modes [4], the relations between source brightness, beam brightness and the degree of coherence have not been thoroughly investigated. Indeed, at least one inconsistency

*) 29, rue Jeanne Marvig, 31055 TOULOUSE CEDEX, France.